The reliability of parameters obtained by fitting of ^{1}H NMRD profiles and ^{17}O NMR data of potential Gd^{3+}-based MRI contrast agents

Peters, Joop A.

DOI
10.1002/cmmi.1677

Publication date
2016

Published in
Contrast Media & Molecular Imaging

Citation (APA)
Peters, J. A. (2016). The reliability of parameters obtained by fitting of ^{1}H NMRD profiles and ^{17}O NMR data of potential Gd^{3+}-based MRI contrast agents. *Contrast Media & Molecular Imaging*, *11*(2), 160-168. https://doi.org/10.1002/cmmi.1677

Full paper

CONTRAST MEDIA & MOLECULAR IMAGING

Received: 27 August 2015, Revised: 2 November 2015, Accepted: 9 November 2015, Published online in Wiley Online Library: 21 December 2015

(wileyonlinelibrary.com) DOI: 10.1002/cmmi.1677

The reliability of parameters obtained by fitting of ^{1}H NMRD profiles and ^{17}O NMR data of potential Gd^{3+}-based MRI contrast agents

Joop A. Peters*

Synthetic variable temperature ^{1}H NMRD profiles and ^{17}O NMR relaxation and shift data were generated with a model based on the Solomon–Bloembergen–Morgan and Freed theories and then fitted simultaneously or individually. The effects of the fitting procedure and of experimental uncertainties on the resulting best-fit parameters were investigated. The most reliable best-fit parameters were obtained when all data were included in a simultaneous fitting procedure. Fitting of only NMRD and/or ^{17}O NMR data provided considerably less accurate best-fit parameters. Very large deviations from the values of the parameters used for the construction of the datasets were obtained due to the combined effects of uncertainties resulting from the fitting and from the data. For these fittings, the accuracy of the best-fit parameters appeared to be strongly dependent on the magnitude of synthetic parameters applied. For example, the accuracy of τ_M^C was low around $\tau_M^S = 10^{-8}$ s. The parameters τ_V and Δ^2 are strongly correlated in fittings of only ^{17}O NMR data. Consequently, only the ratio of these parameters can be evaluated in this way. The observations underline the need to reduce the number of adjustable parameters by constraining as many as possible of them at values obtained by independent techniques. The inaccuracies observed in these simulations come in addition to those caused by the inadequacy of the Solomon–Bloembergen–Morgan theory, particularly at low magnetic field strengths. Copyright © 2015 John Wiley & Sons, Ltd.

Keywords: MRI contrast agents; relaxivity; water exchange rate; rotational correlation times; electronic relaxation times

1. INTRODUCTION

Insight into the parameters that influence the efficacy of contrast agents (CAs) for MRI is essential for the rational design of novel more efficient agents (1–4). The most frequently applied CAs are Gd^{3+}-based compounds, which improve the contrast by enhancing the longitudinal relaxation rates of water protons in their proximity. Their efficacy is usually expressed as the relaxivity (r_1), the longitudinal relaxation rate enhancement normalized to 1 mmol of Gd^{3+}, which is determined by (i) experimental parameters: magnetic field strength (B) and temperature (T), (ii) structural and dynamic parameters of the CA and (iii) physical parameters associated with the electronic relaxation of the Gd^{3+} ion. The relaxivity as a function of the magnetic field strength (the ^{1}H NMRD profile) can be evaluated with models based on the Solomon–Bloembergen–Morgan (SBM) (5–8) and the Freed theory (9) for the inner and outer sphere contributions, respectively. Various refinements of the SBM model have been proposed, which more accurately describe the electronic relaxation (10) and the mobility of the system (11). It should be noted that the SBM model is an approximate theory based on many assumptions and is not generally valid (10,12). However, many groups use this model to evaluate the parameters governing the relaxivity of CAs by fitting their NMRD profiles. Such a fitting is a cumbersome procedure because at least 10 adjustable parameters are required for each temperature. Therefore, constraints are usually introduced by fixing as many adjustable parameters as possible at the most likely values or better at values that have been determined independently. For instance, fitting of the variable temperature ^{17}O NMR relaxation rates (T_1 and T_2) and chemical shifts induced by the CA with a model based on the equations of Swift and Connick (8,13,14) affords values for the residence time of water in the first coordination sphere of Gd^{3+} (τ_M) and electronic relaxation time parameters. The fitting of the NMRD profiles and the ^{17}O data can be performed either separately or simultaneously (8). Further constraints can be applied by including multiple frequency EPR linewidth data in the fitting procedure (8).

A complete physicochemical characterization of a potential CA through the parameters that govern its relaxivity requires collection and analysis of a large amount of data, and therefore is very time consuming. The attention of researchers in the field is shifting from low molecular weight Gd-chelates for non-selective contrast enhancement to complex materials, which allow combination of highly sensitive MRI probes with those for other diagnostic imaging techniques in multiple probes or with therapeutic agents in so-called theranostics. NMRD profiles can be measured with samples having a Gd^{3+} concentration of about 1 mM, but accurate ^{17}O NMR measurements require concentrations that are at least an order of magnitude higher. Unfortunately, such concentrations often cannot be reached for complex materials such as nanoparticles, and variable temperature measurements may also be difficult with these materials.

* *Correspondence to: J. A. Peters, Department of Biotechnology, Delft University of Technology, Julianalaan 136, 2628 BL Delft, The Netherlands. E-mail: J.A.Peters@tudelft.nl*

J. A. Peters
Department of Biotechnology, Delft University of Technology, Julianalaan 136, 2628 BL Delft, The Netherlands

Usually, the inaccuracies of best-fit parameters of experimental relaxation and shift data of CAs are reported as standard deviations as obtained by the fitting algorithm. This may be misleading because these procedures do not take into account inaccuracies due to (i) the invalidity of the assumptions on which the of the SBM model is based and (ii) the presence of multiple local minima in the optimization. The former source of inaccuracies has been studied extensively by the groups of Fries, Merbach and Helm (1,10,12,15). The present study focusses on aspect (ii), particularly on the reliability of best-fit values obtained by simultaneous fittings of various synthetic NMRD profiles and variable temperature ^{17}O NMR relaxation and shift data, compared with those obtained by fitting of exclusively NMRD or ^{17}O NMR data.

2. RESULTS AND DISCUSSION

2.1. Construction of the synthetic datasets

All synthetic data were generated for five τ_M^{298} values in the range typical for potential CAs (10^{-5}–10^{-9} s) and for τ_R^{298} = 10^{-10} and 10^{-8} s, typical values for low and high molecular weight compounds, respectively. ^{1}H NMRD data were calculated for 28 Larmor frequencies (*LF*s) between 0.01 and 400 MHz at 5, 15, 25, 37 and 50 °C and ^{17}O NMR data for 10 temperatures in the range 5–95 °C at a magnetic field strength of 7.05 T. Other parameters used to calculate the data were arbitrarily chosen in the range usually reported for CAs (1) and are tabulated in Table 1. To simulate the effect of inaccuracies in the experimental data, additional synthetic datasets were constructed with random errors of 3% added to the ^{1}H and ^{17}O relaxation rates and 5% added to the ^{17}O chemical shifts.

2.1.1. *Synthetic ^{1}H NMRD data*

The study is limited to the relatively simple situation where second sphere waters are absent and local motions are unimportant. Two contributions are considered to influence the longitudinal proton relaxation rate profile, inner sphere ($r_{1,IS}$) and outer sphere relaxivity ($r_{1,OS}$):

$$r_1 = r_{1,IS} + r_{1,OS} \tag{1}$$

The dipolar interaction dominates $r_{1,IS}$ and is described by eqn (2) (13) and the Solomon–Bloembergen equation (eqn (3)) (5–7), where q is the number of inner sphere water molecules (assumed to be unity in the present calculations) and T_{1M} is the longitudinal relaxation time of a Gd^{3+}-bound water molecule. The distance between Gd^{3+} and the H atom of a bound water molecule (r_{GdH}) was fixed at 3.10 Å, unless stated otherwise.

$$r_{1,IS} = \frac{q}{55556(T_{1M} + \tau_M)} \tag{2}$$

$$\frac{1}{T_{1M}} = \frac{2}{15}\left(\frac{\mu_0}{4\pi}\right)^2 \frac{\hbar^2\gamma_S^2\gamma_I^2}{r_{GdH}^6} S(S+1)\left(\frac{3\tau_{d1}}{1+\omega_I^2\tau_{d1}^2} + \frac{7\tau_{d2}}{1+\omega_S^2\tau_{d2}^2}\right) \tag{3}$$

Here $(\mu_0/4\pi)$ is the magnetic permeability in vacuum, S is the electron spin (S = 7/2 for Gd^{3+}), γ_I is the nuclear gyromagnetic ratio, γ_S is the electron gyromagnetic ratio, ω_I and ω_S are the Larmor frequencies of the proton and electron spin, respectively, and $\tau_{di}^{-1} = \tau_M^{-1} + \tau_R^{-1} + T_{ie}^{-1}$, where T_{ie} (i = 1, 2) stands for electronic relaxation time. The latter are mainly due to the zero field splitting (ZFS) interaction and can be expressed by eqns (4) and (5) (16):

$$\frac{1}{T_{1e}} = \frac{1}{25}\Delta^2\tau_v[4S(S+1)-3]\left(\frac{1}{1+\omega_S^2\tau_v^2} + \frac{1}{1+4\omega_S^2\tau_v^2}\right) \tag{4}$$

$$\frac{1}{T_{2e}} = \Delta^2\tau_v\left(\frac{5.26}{1+0.372\omega_S^2\tau_v^2} + \frac{7.18}{1+1.24\omega_s\tau_v}\right) \tag{5}$$

In these equations, Δ^2 represents the mean-squared fluctuation of the ZFS and τ_v is the correlation time for the instantaneous distortion of the coordination polyhedron of Gd^{3+}.

The outer sphere contribution to the relaxivity ($r_{1,OS}$) is described by eqs (6) and (7) (9):

$$r_{1,OS} = \left(\frac{32\pi}{405}\right)\left(\frac{\mu_0}{4\pi}\right)^2\gamma_I^2\gamma_S^2\hbar^2 S(S+1)\frac{N_A}{a_{GdH}D_{GdH}} [3J_{OS}(\omega_I, T_{1e}) + 7J_{OS}(\omega_S, T_{1e})] \tag{6}$$

$$J_{OS}(\omega, T_{je}) = \mathrm{Re}\left\{\frac{1+\frac{1}{4}\left[i\omega\tau_{GdH} + \left(\frac{\tau_{GdH}}{T_{je}}\right)\right]^{\frac{1}{2}}}{1+\left[i\omega\tau_{GdH} + \left(\frac{\tau_{GdH}}{T_{je}}\right)\right]^{\frac{1}{2}} + \frac{4}{9}\left[i\omega\tau_{GdH} + \left(\frac{\tau_{GdH}}{T_{je}}\right)\right] + \frac{1}{9}\left[i\omega\tau_{GdH} + \left(\frac{\tau_{GdH}}{T_{je}}\right)\right]^{\frac{3}{2}}}\right\} \tag{7}$$

Here N_A is Avogadro's number, a_{GdH} is the distance of closest approach of a diffusing water molecule to Gd^{3+}, which was fixed at 3.5 Å in all calculations, D_{GdH} stands for the diffusion coefficient and $Jos(\omega, T_{je})$ (j = 1, 2) are spin density functions. Generally, D_{GdH} can be well estimated by an empirical equation proposed by Vander Elst *et al.* (17), and consequently this parameter can be fixed in the fitting procedure. In the present calculations D_{GdH}^{298} was arbitrarily set at 2.2×10^{-9} m^2 s^{-1}. The diffusion correlation time (τ_{GdH}) is given by a_{GdH}^2/D_{GdH}. All other correlation times are assumed to obey an exponential temperature dependence (eqn (8)), where x = R, M or V, τ_x^T and τ_x^{298} are the values of the parameter concerned at temperature T and 298.15 K,

Table 1. Values of variables used in calculations of synthetic ^{1}H NMRD and ^{17}O NMR data. The values that were fixed during the fittings are in italic

q	1.0
r_{GdH} (Å)	3.10
τ_M^{298} (s)	10^{-5}–10^{-9}
τ_R^{298} (s)	10^{-8}, 10^{-10}
τ_V^{298} (ps)	15.0
Δ^2 (10^{19} s^{-2})	1.60
D_{GdH}^{298} (10^{-9} m^2 s^{-1})	*2.20*
a_{GdH}^2 (Å)	*3.50*
$A/\hbar$ (10^6 rad s^{-1})	*3.60*
$\chi(1+\eta^2/3)^{1/2}$ (MHz)	*7.58*
r_{GdO} (Å)	*2.50*
C_{OS}	*0.1*
E_M (kJ mol^{-1})	47.6
E_R (kJ mol^{-1})	21.9
E_V (kJ mol^{-1})	*1.0*
E_D (kJ mol^{-1})	*18.2*

respectively, E_x is the associated activation energy and R is the gas constant.

$$\tau_x^T = \tau_x^{298} \exp\left[\frac{E_x}{R}\left(\frac{1}{T} - \frac{1}{298.15}\right)\right] \quad (8)$$

The temperature dependence of D_{GdH} is assumed to obey

$$D_{GdH}^T = D_{GdH}^{298} \exp\left[\frac{E_D}{R}\left(\frac{1}{298.15} - \frac{1}{T}\right)\right] \quad (9)$$

E_v was fixed at 1.0 kJ mol^{-1} and E_D at 18.2 kJ mol^{-1}.

2.1.2. *Synthetic ^{17}O NMR data*

Synthetic datasets consisting of reduced Gd^{3+}-induced water ^{17}O longitudinal and transverse relaxation rates ($1/T_{1r}$ and $1/T_{2r}$) and angular frequencies ($\Delta\omega_r$) were generated using eqns (10–12):

$$\frac{1}{T_{1r}} = \frac{1}{T_{1M} + \tau_M} \quad (10)$$

$$\frac{1}{T_{2r}} = \frac{1}{\tau_M}\frac{T_{2M}^{-2} + \tau_M^{-1}T_{2M}^{-1} + \Delta\omega_M^2}{\left(\tau_M^{-1} + T_{2M}^{-1}\right)^2 + \Delta\omega_M^2} \quad (11)$$

$$\Delta\omega_r = \frac{\Delta\omega_M}{\left(1 + \tau_M T_{2M}^{-1}\right)^2 + \tau_M^2\Delta\omega_M^2} + C_{OS}\Delta\omega_M \quad (12)$$

The outer sphere contributions to the relaxation rates have been shown to be negligible (18), and therefore are not included in eqns (10) and (11). The outer sphere contribution to $\Delta\omega_r$ is assumed to be proportional to $\Delta\omega_M$ and is represented by the last term in eqn (12). The constant C_{OS} was fixed at 0.1 in the present calculations. The ^{17}O longitudinal relaxation rates in eqn (10) are dominated by contributions of the dipole–dipole and quadrupolar mechanisms as expressed by eqns (13–16) (16):

$$\frac{1}{T_{1M}} = \frac{1}{T_{1dd}} + \frac{1}{T_{1q}} \quad (13)$$

$$\frac{1}{T_{1dd}} = \frac{1}{15}\frac{\gamma_I^2\gamma_S^2\hbar^2}{r_{GdO}^6}S(S+1)\left(\frac{\mu_0}{4\pi}\right)^2\left[6\tau_{d1} + 14\frac{\tau_{d2}}{1+\omega_S^2\tau_{d2}^2}\right] \quad (14)$$

$$\frac{1}{T_{1q}} = \frac{1}{T_{2q}} = \frac{3\pi^2(2I+3)}{10I^2(2I-1)}\chi^2\left(1+\eta^2/3\right)\tau_{RO} \quad (15)$$

$$\tau_{di}^{-1} = \tau_M^{-1} + \tau_{RO}^{-1} + T_{ie}^{-1} \quad i = 1,2 \quad (16)$$

Here, r_{GdO} is the distance between the electron charge and the ^{17}O nucleus, which was fixed at 2.50 Å in the present calculations. The rotational correlation time for the Gd–O vector (τ_{RO}) is not necessarily equal that of the Gd–water H vector, τ_{RH} (19). In the present calculations, the ratio τ_{RO}/τ_{RH} was fixed at 1.54. In eqn (15), χ is the quadrupolar coupling constant and η an asymmetry parameter. The value of the quadrupole coupling parameter $\chi\sqrt{(1 + \eta^3/3)}$ was set at the value of pure water, 7.58 MHz (20,21).

$1/T_{2q}$ is equal to $1/T_{1q}$ (see eqn (15)) and the scalar and dipolar contributions to the transverse ^{17}O relaxation rate are given by eqns (17) and (18), (19), respectively:

$$\frac{1}{T_{2SC}} = \frac{S(S+1)}{3}\left(\frac{A}{\hbar}\right)^2\tau_{e1} \quad (17)$$

$$\frac{1}{T_{2dd}} = \frac{1}{15}\frac{\gamma_I^2\gamma_S^2\hbar^2}{r_{GdO}^6}S(S+1)\left(\frac{\mu_0}{4\pi}\right)^2\left[7\tau_{d1} + 13\frac{\tau_{d2}}{1+\omega_S^2\tau_{d2}^2}\right] \quad (18)$$

$$\tau_{e1}^{-1} = \tau_M^{-1} + T_{1e}^{-1} \quad (19)$$

$$\frac{1}{T_{2M}} = \frac{1}{T_{2dd}} + \frac{1}{T_{2q}} + \frac{1}{T_{2SC}} \quad (20)$$

Micskei *et al.* have determined that, for $[Gd(DTPA)(H_2O)]^{2-}$ and for $[Gd(DOTA)(H_2O)]^{-}$, the scalar contribution makes up 95% of $1/T_{2M}$, and therefore, in their calculations, the contributions of the dipolar and the quadrupolar relaxation mechanisms could be neglected (18). Generally, in fittings of ^{17}O NMR relaxation rates, the dipolar and quadrupolar contributions are neglected as well (1). However, simulations show that for systems with smaller τ_M and/or larger τ_R this assumption is no longer valid. For example, for $LF = 40$ MHz, $\tau_M = 1$ ns, $\tau_R = 1$ ns and with the other parameters the same as for $[Gd(DTPA)(H_2O)]^{2-}$, the dipolar, scalar and quadrupolar contributions to $1/T_{2M}$ are 27, 54 and 19%, respectively. Therefore, in the present calculations, all these contributions are included in $1/T_{2M}$ (see eqn (20)).

2.2. Fittings of the synthetic datasets

2.2.1. *Procedures*

The fittings were carried out by minimization of S^2, the sum of the squared differences between calculated and synthetic data (see eqn (21)) using the evolutionary algorithm of the Microsoft Excel Solver (22). This algorithm has the advantage that it results usually in a global minimum. Initial estimates of the fitting parameters were randomly generated numbers within the ranges commonly observed for these parameters (see Table S1). The minimization procedure was continued until no further significant decrease of S^2 occurred after restarting. For display purposes, the goodness of the fits was expressed as the agreement factor (*AF*; see eqn (22)). The final values of S^2 and *AF* were always below those calculated for the synthetic data after adding the random errors with respect to synthetic data without added errors ($AF \leq 0.02$). Standard deviations of the best-fit parameters were calculated by repeating a minimization five times with different randomly generated initial estimates.

$$S^2 = \sum_i \left(y_i^c - y_i^s\right)^2 \quad (21)$$

$$AF = \sqrt{\frac{\sum_i \left(y_i^c - y_i^s\right)^2}{\sum_i \left(y_i^s\right)^2}} \quad (22)$$

The fittings of the synthetic data were carried out with four different methods:

(A) variable temperature NMRD data and ^{17}O NMR data simultaneously;

Table 2. Comparison of parameters used for the construction of synthetic variable temperature ^{1}H NMRD data with best-fit parameters obtained from this dataset with Method B

	Synthetic[1]	Best-fit parameters		
		No errors[2,3]	Errors included[2]	
			Minimum 1	Minimum 2
τ_M^{298} (s)	10^{-9}	$(2.1 \pm 0.1) \times 10^{-9}$	$(1.5 \pm 0.5) \times 10^{-7}$	$(3 \pm 2) \times 10^{-9}$
τ_R^{298} (ps)	100.0	95.0 ± 0.3	90.0 ± 0.8	93 ± 3
τ_V^{298} (ps)	15.0	15.0 ± 0.0	14.1 ± 0.4	15.5 ± 0.1
Δ^2 (10^{19} s^{-2})	1.60	1.59 ± 0.00	1.38 ± 0.05	1.50 ± 0.01
E_M (kJ mol^{-1})	47.6	56.9 ± 0.9	7 ± 1	53 ± 5
E_R (kJ mol^{-1})	21.9	22.9 ± 0.1	26.0 ± 0.4	23.3 ± 0.8
AF	0.0	2.4×10^{-4}	2.1×10^{-2}	2.2×10^{-2}

[1]All other parameters were fixed at the values given in Table 1. The best-fit values are averages of results of five fittings with different initial parameters.
[2]In synthetic data.
[3]A single minimum was found.

(B) exclusively the variable temperature NMRD data;
(C) exclusively an NMRD profile for 25 °C;
(D) exclusively variable temperature ^{17}O NMR data.

In all cases excellent fits were obtained with $AF \leq 0.02$. Below, the parameters employed for the construction of the datasets, the "synthetic parameters", will be denoted with a superscript S and those obtained after fitting of these data with a superscript C.

2.2.2. *Method A: simultaneous fitting of variable temperature ^{1}H NMRD and ^{17}O NMR data*

Fittings of synthetic data for $\tau_M^{298S} = 10^{-5}$–10^{-9} s and $\tau_R^{298S} = 10^{-10}$ s afforded best-fit parameters that were always within 0.1% of the values employed for their construction (see Table S2). The standard deviations were negligibly small.

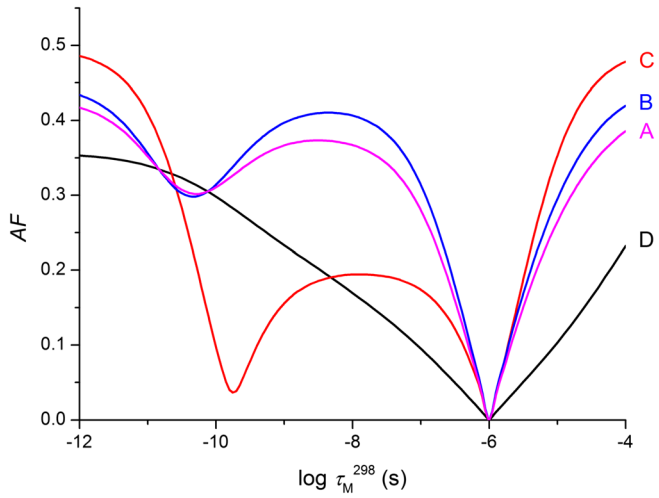

Figure 1. Plot of *AF* versus log τ_M^{298} for the various fitting procedures of synthetic datasets constructed for $\tau_M^{298S} = 10^{-6}$ s, $\tau_R^{298S} = 10^{-10}$ s and the other parameters fixed at the values mentioned in Table 1.

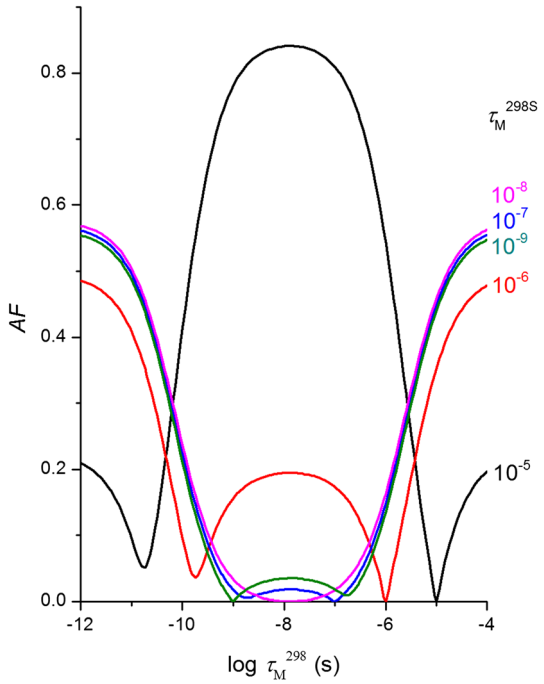

Figure 2. Plot of *AF* versus log τ_M^{298} for fitting of synthetic NMRD datasets (Procedure C) constructed for various values of τ_M^{298S}, with the other parameters fixed at the values mentioned in Table 1.

2.2.3. *Method B: fitting of variable temperature ^{1}H NMRD data*

Fittings of synthetic NMRD data for $\tau_M^{298S} = 10^{-5}$–10^{-8} s and $\tau_R^{298S} = 10^{-10}$ s again all resulted in excellent fits ($AF < 10^{-4}$), and produced best-fit parameters that were identical to the corresponding synthetic values and that had negligible standard deviations (see Table S4). However, for $\tau_M^{298S} = 10^{-9}$ s, τ_M^{298C} deviated by a factor of about 2 from the corresponding synthetic values and had relatively large standard errors (see Table 2), although the fit was still perfect ($AF = 2 \times 10^{-4}$). The deviations in τ_M were mainly compensated by small changes in τ_R and E_M.

Table 3. Comparison of parameters used for the construction of synthetic variable temperature ^{17}O NMR data with best-fit parameters obtained from this dataset with Method D. Standard deviations are given in parentheses[1]

	Synthetic	Best-fit parameters	
		No errors[2]	Errors included[2]
τ_M^{298} (μs)	1.00	1.00 (0.00)	0.99 (0.00)
τ_R^{298} (ps)	100.0	100.0 (0.0)	100.9 (0.0)
τ_V^{298} (ps)	15.0	70 (13)	58 (13)
Δ^2 (10^{19} s^{-2})	1.60	7.5 (1.4)	5 (1)
E_M (kJ mol^{-1})	47.6	47.6 (0.0)	47.9 (0.0)
E_R (kJ mol^{-1})	21.9	21.9 (0.0)	22.3 (0.0)
Δ^2/τ_V^{298} (10^{30} s^{-3})	1.0667	1.06 (0.00)	1.02 (0.00)
AF	0.0	7.4×10^{-7}	1.6×10^{-3}

[1]All other parameters were fixed at the values given in Table 1. The best-fit values are averages of results of five fittings with different initial parameters.
[2]In synthetic data.

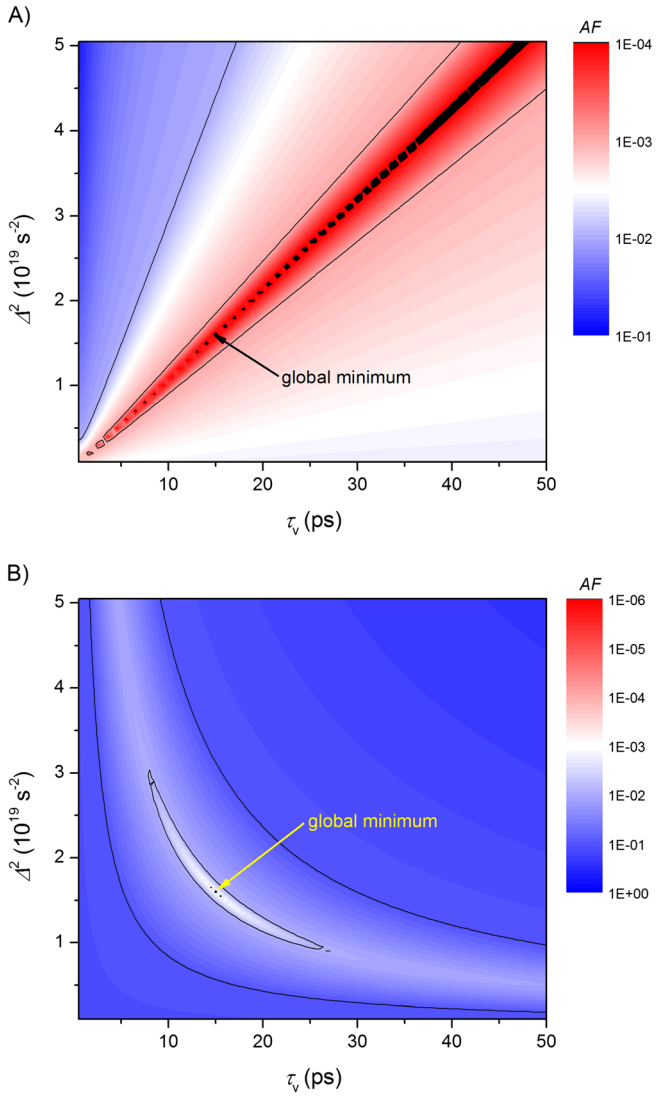

Figure 3. Contour plot of *AF* for a synthetic dataset with $\tau_M^{298S} = 1$ μs, as a function of τ_V^{298} and Δ^2 for (A) fitting of ^{17}O data (Procedure D) and (B) fitting variable temperature NMRD data (Procedure B).

This decrease in accuracy of τ_M^{298C} can be ascribed to the transition of the water exchange rate from the slow to the fast exchange limit. For $\tau_M^{298} = 10^{-9}$ s, the fast exchange limit is reached and τ_M is so small relative to T_{1M} that it can be neglected in eqn (2). Consequently, τ_M influences r_1 only through the correlation times that govern T_{1M}, namely τ_{d1} and τ_{d2}, which are given by $\tau_{di}^{-1} = \tau_M^{-1} + \tau_R^{-1} + T_{ie}^{-1}$. In the NMRD profiles concerned, the relaxivity contribution due to electronic relaxation dominates up to $LF \approx 1$ MHz, whereas the effects of τ_M and τ_R dominate at 1–100 MHz. Thus in the latter *LF* region, deviations of τ_M^C from τ_M^S are mainly reflected in variations in the shape of the NMRD profile at 1–100 MHz, which can be compensated optimally by variations in τ_R^C and vice versa. The sum of the reciprocals of these correlation times of each fitting was the same as that of the corresponding synthetic values τ_M^S and τ_R^S.

2.2.4. *Method C: fitting of only ^1H NMRD data for 25 °C*

An inspection of *AF* curves for fittings of synthetic NMRD datasets for a single temperature (Procedure C) as a function of τ_M^{298} shows that next to the global minimum a local minimum is present with a slightly higher *AF* (see Fig. 1). This can be explained by the shape of curves of the relaxivity r_1 as a function of τ_M. From eqns (2–5) it can be deduced that at a particular *LF* such a curve presents a maximum when $T_{1M}^{-1} < \tau_M^{-1} < \tau_R^{-1}$; T_{1e}^{-1} (1). Hence, below this maximum, a given value of r_1 corresponds to two values of τ_M, which are located opposite each other with respect to the maximum. For the datasets without included random errors, the fitting procedures always ended always in the proper minimum for *AF*, when the evolutionary algorithm was applied for the minimization. Near the value of τ_M, where the maxima in r_1 occur ($\tau_M^{298} \approx 10^{-8}$ s), the two minima in the curve for *AF* overlap (see Fig. 2), and consequently τ_M^C had larger standard deviations and differed substantially from τ_M^S (see also Table S6).

For $\tau_M^{298S} = 10^{-5}$ s, the best-fit value τ_R^{298C} appeared to be a factor of 10 higher than its synthetic counterpart. This can be rationalized by eqn (2), where τ_M is larger than T_{1M} under these conditions, whereas at the same time it is of minor importance in τ_{di} (see eqn (3)). As a result, small deviations in τ_M have to be compensated by relatively large deviations in the other fitting parameters to reach a good fit.

2.2.5. *Method D: fitting of only variable temperature ^{17}O NMR data*

If only ^{17}O NMR data were considered, the evaluated best-fit values for the parameters governing the electronic relaxation (τ_V^{298} and Δ^2) deviated substantially from the corresponding synthetic values, whereas the best fits of all other parameters were perfectly in agreement with the corresponding synthetic values. This is illustrated in Table 3 for $\tau_M^{298S} = 10^{-6}$ s (see also Table S8). Although the fittings did not afford the correct values for τ_V^{298} and Δ^2, the qualities of the fits were excellent, as reflected in very low values for *AF*. A contour plot of *AF* as a function of τ_V^{298} and

Table 4. Comparison of best-fit parameters for synthetic data constructed with $\tau_M^{298S} = 10^{-7}$ s and $\tau_R^{298S} = 10^{-10}$ s as obtained with Procedures A–D. Random errors were included in the data

	Synthetic	A	B	C	D
τ_M^{298} (s)	1.00×10^{-7}	$(1.04 \pm 0.00) \times 10^{-7}$	$(2.9 \pm 0.7) \times 10^{-7}$	$(1.3 \pm 1.0) \times 10^{-7}$	$(0.99 \pm 0.00) \times 10^{-7}$
τ_R^{298} (ps)	100.0	100.1 ± 0.0	104 ± 2	106 ± 3	98.4 ± 0.0
τ_V^{298} (ps)	15.0	16.2 ± 0.0	14.6 ± 0.9	10 ± 4	57 ± 16
Δ^2 (10^{19} s^{-2})	1.60	1.49 ± 0.00	1.36 ± 0.02	2.9 ± 0.8	6 ± 2
E_M (kJ mol^{-1})	47.6	48.5 ± 0.0	28 ± 5	–	47.6 ± 0.0
E_R (kJ mol^{-1})	21.9	21.9 ± 0.0	23.8 ± 0.7	–	21.7 ± 0.0
AF	0.0	0.017	0.019	0.025	0.002

Δ^2 (see Fig. 3) shows a valley with local minima along the line $\Delta^2 \approx 1.1 \times 10^{30} \tau_V^{298}$ (see Fig. 3(A)). Inside this valley a global minimum occurs at $\tau_V^{298} = 15$ ps, $\Delta^2 = 1.6 \times 10^{19}$ s^{-2} (AF = 7.5×10^{-6}), which was missed in the fitting procedure, due to the shallowness of the curve along the minima. The strong correlation between τ_V^{298} and Δ^2 can be explained by consideration of eqns (4) and (5). At the magnetic field strengths usually applied for ^{17}O NMR (in the present example $B = 7.04$ T), the term $\omega_S\tau_V$ is larger than unity. After filling in all the physical constants, it can be seen that both $1/T_{1e}$ and $1/T_{2e}$ are approximately proportional to Δ^2/τ_V. Consequently, fitting of the ^{17}O NMR data can be used to get an estimate only of the ratio Δ^2/τ_V rather than of the individual parameters (see Table 3). By contrast, the part of the NMRD profiles for $B < 1$ T is mainly determined by the electronic relaxation rates, and at these magnetic field strengths the approximations mentioned above are no longer valid. Accordingly, there is no correlation between τ_V^{298} and Δ^2 and thus a good estimate of both parameters can be obtained from fitting of ^{1}H NMRD (Method B or C) data alone or simultaneously with the ^{17}O NMR data (Method A; see Fig. 3(B)).

2.2.6. *Effects of inclusion of random errors in the synthetic data*

Inclusion of random errors of 3% in the relaxation rates and of 5% in the chemical shifts had a relatively small magnifying effect on the inaccuracy of the best-fit data obtained with a simultaneous fit (Method A): all best-fit parameters were within 10% of their synthetic values. However, smaller datasets (Methods B–D) afforded best-fit values that deviated substantially and had relatively large standard deviations, although excellent fits were always obtained irrespective of the procedure employed (see Tables S2–S9). This is illustrated for the best-fit parameters for the datasets for $\tau_M = 10^{-7}$ s in Table 4, whereas in Fig. 4 the curves calculated with the values obtained with Procedure A are displayed.

As expected based on the results mentioned in the previous section, the fittings of only ^{17}O NMR data gave unreliable best-fit values for τ_V^{298} and Δ^2, but values close to the synthetic ones were obtained for τ_M^{298}, τ_R^{298} and the activation energies. The opposite holds for the fittings of NMRD data only. Fittings of the NMRD dataset constructed for $\tau_M^{298} = 10^{-9}$ s ended up in one of the two *AF* minima. In this case the minimizations were repeated until five of each of the minima were obtained. In most cases, the global minimum could be identified by a careful inspection of a plot of *AF* as a function of τ_M^{298}. However, great care is needed, since the differences between the *AF* values of the two minima are always very small. If possible, either the temperature dependence of NMRD data or ^{17}O NMR data should be used to discriminate between the two minima.

The plots of *AF* as function of τ_M^{298} almost coincided with the corresponding plot shown in Fig. 2; only the lower part of the curve was shifted upward by about 0.02 *AF* units. Consequently, the separation of the two local minima was less than prior to the inclusion of random errors in the synthetic dataset. This flattening of the minima leads to a larger spreading of the best-fit values for the results of individual fittings, as reflected in the relatively large standard deviations for the best-fit values of τ_M^{298C} for datasets constructed with $\tau_M^{298S} = 10^{-7}$–10^{-9} s (see Table S5).

2.2.7. *Synthetic datasets for $\tau_R^{298S} = 10^{-8}$ s*

Upon increase of τ_R^{298S}, the valleys in the profiles of *AF* as a function of τ_R become narrower. Consequently, the values of the best-fit parameters are closer to those of the parameters used to construct the synthetic datasets, and their standard deviation generally decreases (compare Tables 5 and 4). When Procedure C is

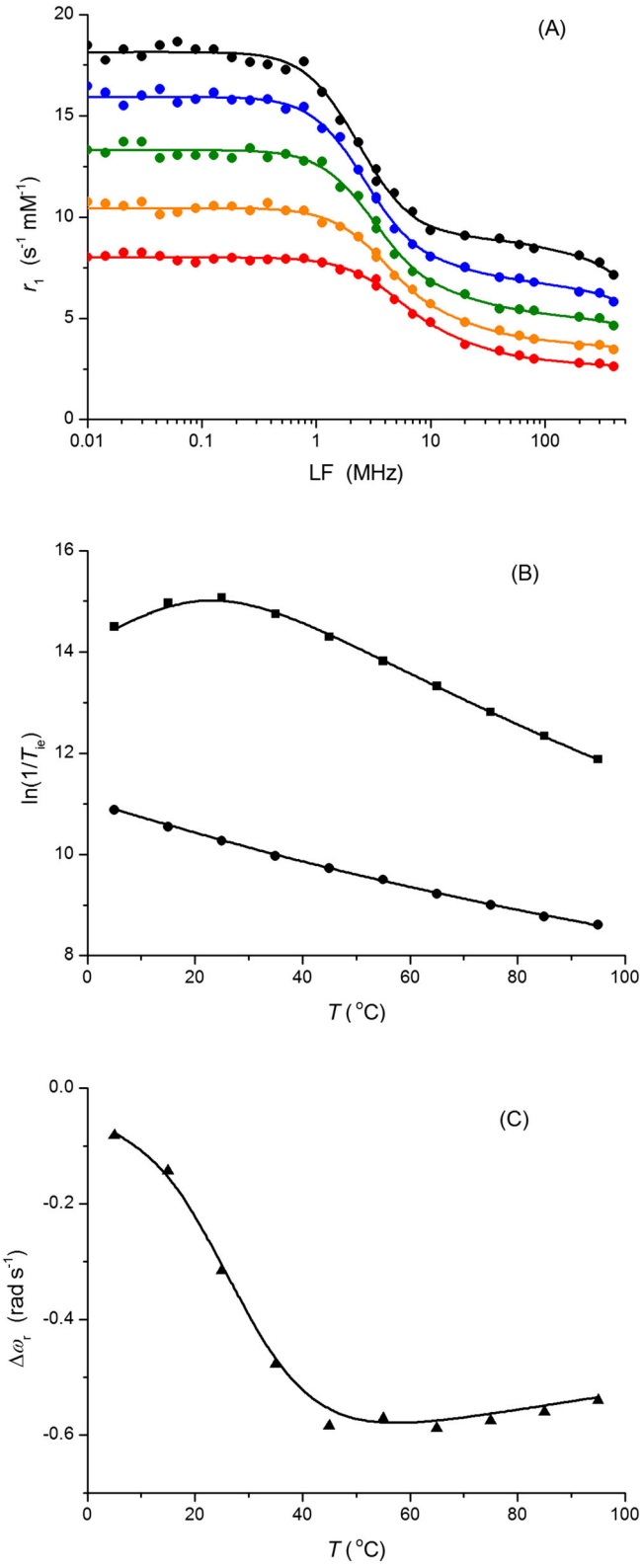

Figure 4. Results of simultaneous fitting of synthetic datasets using the best-fit values given in Table 4, Procedure A. (A) ^{1}H NMRD data for 5 (black), 15 (blue), 25 (green), 37 (orange) and 50 °C (red); (B) reduced ^{17}O NMR relaxation rates (■, $1/T_{2r}$; ●, $1/T_{1r}$); (C) reduced ^{17}O NMR chemical shifts of water.

Table 5. Comparison of best-fit parameters for synthetic data constructed with $\tau_M^{298S} = 10^{-7}$ s and $\tau_R^{298S} = 10^{-8}$ s as obtained with Procedures A–D

	Synthetic	A	B	C	D
τ_M^{298} (s)	1.00×10^{-7}	$(1.01 \pm 0.00) \times 10^{-7}$	$(1.01 \pm 0.00) \times 10^{-7}$	$(1.03 \pm 0.00) \times 10^{-7}$	$(1.00 \pm 0.00) \times 10^{-7}$
τ_R^{298} (s)	10^{-8}	$(0.98 \pm 0.01) \times 10^{-8}$	$(0.98 \pm 0.02) \times 10^{-8}$	$(0.94 \pm 0.01) \times 10^{-8}$	$(1.00 \pm 0.00) \times 10^{-8}$
τ_V^{298} (ps)	15.0	15.0 ± 0.0	15.0 ± 0.0	15.0 ± 0.0	43 ± 18
Δ^2 (10^{19} s^{-2})	1.60	1.60 ± 0.00	1.59 ± 0.01	1.59 ± 0.01	4 ± 2
E_M (kJ mol^{-1})	47.6	48.0 ± 0.1	47.9 ± 0.2	–	47.7 ± 0.0
E_R (kJ mol^{-1})	21.9	22.0 ± 0.0	22.2 ± 0.4	–	21.9 ± 0.0
AF	0.0	0.020	0.021	0.021	0.0015

applied, the separation between the two local minima is better. Then, the global minimum can be located more easily. This is illustrated in Fig. 5, which displays the profiles for $\tau_R = 10^{-8}$ and 10^{-10} s.

2.2.8. *Variation of q and r_{GdH}*

From eqn (2), it is evident that evaluation of NMRD data can provide the value of the ratio q/r_{GdH}^6, but not that of either q or r_{GdH}. The parameters q and r_{GdH} are often both fixed in fitting procedures of NMRD data. Determination of either of these parameters from NMRD data requires an independent determination of the other parameter by a different technique.

The value of q can be estimated from the Gd^{3+} induced shift of the water ^{17}O nucleus, provided that the exchange between bound and bulk water is fast on the ^{17}O NMR time scale. This shift is purely of contact origin and is, to a first approximation, linearly proportional to q (23,24). A widely used alternative method to estimate q values of Gd^{3+} complexes is from q values of corresponding Eu^{3+} and/or Tb^{3+} complexes as determined by their luminescence decay rates in H_2O and D_2O (25). A double check of the correctness of a q value can be obtained by fitting NMRD and/or ^{17}O NMR data according to Procedures A or D, by including $A/\hbar$ in the set of adjustable fitting parameters. A best-fit value obtained for $A/\hbar$ in the range from -4.1×10^{-6} to -3.6×10^{-6} rad s^{-1} is an indication that the assumed q value is correct, since the value of $A/\hbar$ is generally almost independent of the structure of the lanthanide complex. Sometimes non-integral numbers have been obtained for q, which may be due to, for example, (i) occurrence of equilibria of Gd-complexes with different hydration states, (ii) neglect of second hydration sphere effects when q was determined by luminescence or (iii) $A/\hbar$ values outside the common range when the ^{17}O NMR method was used. When non-integral q values occur, reliable fittings of NMRD data can only be obtained if the thermodynamic parameters of the hydration equilibria are known. A good estimate can usually be obtained by high resolution UV–vis spectrometric measurements on the corresponding Eu^{3+} system. The intensity of the absorption band for the $^7F_0 \rightarrow {}^5D_0$ transition is low, but generally so narrow that deconvolution into bands for the different hydration states is possible (26–29).

Since the number of required adjustable parameters in fittings is very large, the value of r_{GdH} is often fixed in fittings of NMRD data reported in the literature. Caravan *et al.* have determined the value of r_{GdH} for several Gd-based CAs from anisotropic hyperfine constants as determined by pulsed ENDOR spectroscopy on glassy methanol–water samples (30,31). These distances were all found to be in the narrow range of 3.0–3.2 Å. This seems to justify fixing of r_{GdH} at 3.10 Å. However, some caution is needed, because r_1 is very sensitive to variations of r_{GdH} due to the proportionality of the inner sphere relaxation rate to r_{GdH}^{-6} (see eqn (3)). Table 6 shows that fixing of r_{GdH} at an incorrect value

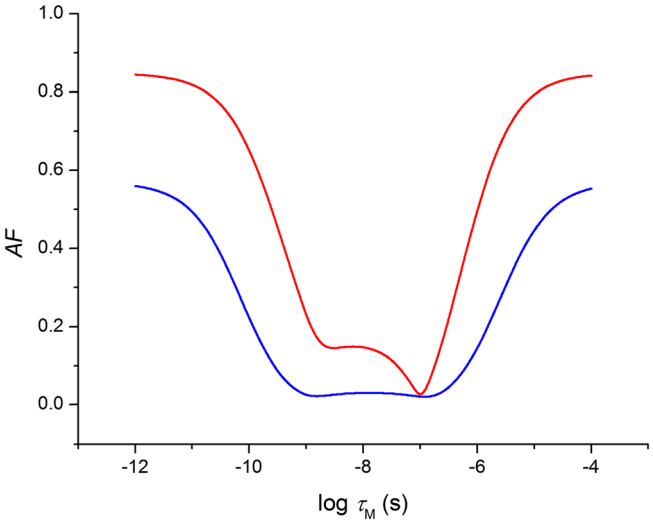

Figure 5. Profiles of AF as function of log τ_M at 25 °C for fittings (Procedure C) of a synthetic NMRD dataset constructed with $\tau_M^{298} = 10^{-7}$ s and $\tau_R = 10^{-8}$ s (red) and 10^{-10} s (blue). All other parameters are as in Table 1. Random errors were included in the synthetic datasets.

Table 6. Best-fit parameters (Procedure D) for synthetic NMRD data constructed with $r_{GdH}^S = 3.10$ Å obtained for various fixed values of r_{GdH}[1]

	Synthetic	Best-fit parameters for r_{GdH} fixed at		
	r_{GdH} = 3.10 Å	3.00 Å	3.10 Å	3.20 Å
τ_M^{298} (10^{-8} s)	1.00	0.08 ± 0.05	0.42 ± 0.40	77.4 ± 0.2
τ_R^{298} (10^{-10} s)	10^{-10}	138 ± 305	1.03 ± 0.02	0.93 ± 0.00
τ_V^{298} (ps)	15.0	21.9 ± 0.0	15.0 ± 0.0	6.6 ± 0.1
Δ^2 (10^{19} s^{-2})	1.60	1.00 ± 0.00[2]	1.61 ± 0.00	2.04 ± 0.04
AF		0.017	0.0055	0.0071

[1]No random errors were included in the synthetic dataset.
[2]Equal to lower boundary imposed on Δ^2 during fitting.

has rather dramatic consequences for the resulting best-fit parameters. On the other hand the −6 power relationship also means that fitting of NMRD data with inclusion of r_{GdH} in the adjustable parameters while q is fixed at a known value reproduces the value of r_{GdH} exactly (see Table S10).

A complicated situation occurs for systems with very fast water exchange rates. For both dissociative and associative water exchange mechanisms, minimal τ_M values and hence minimal activation energies may be expected when the energy difference between the two hydration states involved is small (1). Then, both hydration states may be populated, resulting in non-integral q values. In this situation the Gd–water bond is weakened and accordingly the Gd–O bond may be longer than usual (32), which in turn will have an effect on the value for $A/\hbar$ for the Gd-bound water O atom. When this parameter is not known, ^{17}O NMR cannot provide a value for q.

2.2.9. *Beyond the approximate SBM theory*

The above data were all generated and fitted with the simplest form of the SBM theory, which is the only theory leading to analytical equations. In reality it has been shown that the SBM theory is not generally valid (1,10,12,15). Especially at low frequencies at which transverse electronic relaxation is important, the SBM approximation in general does not lead to correct results, particularly not for the electronic relaxation parameters. Therefore, many researchers now fit ^{1}H NMRD data only for $LF \geq 10$ MHz. Some fittings were performed on the datasets discussed above after deleting the ^{1}H NMRD data for $LF < 10$ MHz (see Table 7). The best-fit parameters obtained for the dataset for $\tau_M^{298S} = 10^{-7}$s and $\tau_R^{298S} = 10^{-10}$ s deviate substantially from the corresponding synthetic parameters. An inspection of the profiles of AF as a function of the various parameters shows that no minima occur in the profiles for the electronic parameters (τ_V^{298} and Δ^2) within the boundaries set on these parameters during the fitting procedure (10^{-12} s $< \tau_V^{298} < 10^{-10}$ s; 10^{19} s$^{-2} < \Delta^2 < 2 \times 10^{20}$ s^{-2}). This is due to the low contribution of the electronic relaxation time to the correlation time τ_{di} for the selected rotational correlation time ($\tau_R^{298S} = 10^{-10}$ s). The inaccuracy is obviously enhanced by the small number of ^{1}H NMRD data points available at $LF < 10$ MHz. By contrast, the dataset generated for $\tau_M^{298S} = 10^{-7}$ s and $\tau_R^{298S} = 10^{-8}$ s resulted in best-fit parameters that are in good agreement with the corresponding synthetic parameters. This can be rationalized by the relative importance of T_{ie} in τ_{di} at slow rotation.

3. CONCLUSIONS

The fitting of synthetic datasets described demonstrates that simultaneous fitting of NMRD and ^{17}O data results in the most reliable best-fit parameters. When only ^{17}O NMR data are fitted, a strong correlation between τ_v and Δ^2 prevents determination of these parameters individually, although an accurate estimation of the ratio τ_v/Δ^2 is still possible. The quality of the best-fit parameters depends strongly on the magnitudes of the various parameters, particularly on τ_M. For example, fitting of NMRD data for a single temperature (Method C) gives two local minima of AF as function of τ_M, located symmetrically with respect to the value that gives rise to the τ_M value for which r_1 as function τ_M of would be maximal. The separation of the two local minima decreases upon approaching the latter maximum, and therefore the accuracy of the best-fit parameter and its deviation of τ_M^S decrease as well. For $\tau_R > 10^{-8}$ s, r_1 is rather insensitive for changes in this parameter, and therefore a reliable determination by fitting is impossible. Plots of AF as a function of the various adjustable parameters may be very helpful for the identification of the global minimum and to get an impression of the accuracy of the best-fit parameters. In general, the accuracy of the fitting can be improved by reduction of the number of adjustable parameters by fixing them at values independently determined by other techniques. DFT calculations are emerging as an important tool to accurately predict the various parameters governing the relaxivity of CAs, including q, τ_M, r_{GdH} and $A/\hbar$ (32). Ultimately, combination of these calculations with fitting of experimental data may be an attractive approach to obtain more insight into the relation between structure and relaxivity.

The synthetic datasets described above were calculated for a very simple model. Local mobility and the presence of second sphere water molecules were not taken into account. If these

Table 7. Comparison of best-fit parameters for synthetic data constructed with $\tau_M^{298S} = 10^{-7}$ s and $\tau_R^{298S} = 10^{-10}$ or 10^{-8} s as obtained with Procedures A–D. The NMRD data for $LF < 10$ MHz were excluded during the fittings. Random errors were included in the data

	Synthetic	A	B	C	D
τ_R^{298} (ps)	100.0	99.9 ± 0.0	101.5 ± 0.2	274 ± 3	98.4 ± 0.0
τ_M^{298} (s)	1.00×10^{-7}	$(1.00 \pm 0.00) \times 10^{-7}$	$(1.76 \pm 0.09) \times 10^{-7}$	$(3.24 \pm 0.01) \times 10^{-7}$	$(0.99 \pm 0.00) \times 10^{-7}$
τ_V^{298} (ps)	15.0	73.1 ± 0.3	69 ± 2	1.49 ± 0.03	57 ± 16
Δ^2 (10^{19} s^{-2})	1.60	4.95 ± 0.02	4.5 ± 0.2	4.2 ± 0.1	5 ± 2
E_M (kJ mol^{-1})	47.6	48.1 ± 0.0	36 ± 1	–	47.6 ± 0.0
E_R (kJ mol^{-1})	21.9	21.5 ± 0.0	22.1 ± 0.0	–	21.7 ± 0.0
AF	0.0	0.008	0.013	0.014	0.002
τ_R^{298} (s)	1.00×10^{-8}	$(0.95 \pm 0.00) \times 10^{-8}$	$(0.95 \pm 0.00) \times 10^{-8}$	$(0.91 \pm 0.00) \times 10^{-8}$	$(1.00 \pm 0.00) \times 10^{-8}$
τ_M^{298} (s)	1.00×10^{-7}	$(1.02 \pm 0.00) \times 10^{-7}$	$(1.02 \pm 0.00) \times 10^{-7}$	$(1.06 \pm 0.00) \times 10^{-7}$	$(1.00 \pm 0.00) \times 10^{-7}$
τ_V^{298} (ps)	15.0	15.6 ± 0.0	15.6 ± 0.0	16.1 ± 0.0	43 ± 18
Δ^2 (10^{19} s^{-2})	1.60	1.60 ± 0.00	1.60 ± 0.00	1.62 ± 0.0	4 ± 2
E_M (kJ mol^{-1})	47.6	48.5 ± 0.0	48.6 ± 0.0	–	47.7 ± 0.0
E_R (kJ mol^{-1})	21.9	21.6 ± 0.0	21.6 ± 0.0	–	21.9 ± 0.0
AF	0.0	0.019	0.020	0.014	0.002

phenomena have to be considered, additional adjustable parameters are needed in the fitting procedure, which further reduce the reliability of the best-fit parameters.

Furthermore, it should be noted that the best-fit values of τ_V and Δ^2 often are physically not very meaningful due to (i) the strong correlation between these parameters in ^{17}O relaxation data and (ii) the inadequacy of the SBM theory for the description of the electronic relaxation, particularly at low magnetic field strengths. Physically meaningful values for these parameters can only be evaluated if EPR data are included and if more advanced models are used to describe the electronic relaxation (15). However, a wealth of data has been published in the literature, which has been evaluated by applying the SBM theory on NMR data only. The trends in these data are generally consistent and have been appeared to be very useful for the rational design of more efficient CAs. The values of the electronic parameters obtained in this way should however be considered as effective rather than as physically meaningful.

REFERENCES

1. Tóth É, Helm L, Merbach A. Relaxivity of gadolinium(III) complexes: theory and mechanism. In Chemistry of Contrast Agents in Medical Magnetic Resonance Imaging (2nd edn), Tóth É, Helm L, Merbach A (eds). Wiley: Chichester UK, 2013; 25–81.
2. Caravan P, Ellison JJ, McMurry TJ, Lauffer RB. Gadolinium(III) chelates as MRI contrast agents: structure, dynamics, and applications. Chem Rev 1999; 99(9): 2293–2352.
3. Lopez-Cebral R, Martin-Pastor M, Seijo B, Sanchez A. Progress in the characterization of bio-functionalized nanoparticles using NMR methods and their applications as MRI contrast agents. Prog Nucl Magn Reson Spectrosc 2014; 79: 1–13.
4. Pierre VC, Allen MJ, Caravan P. Contrast agents for MRI: 30+ years and where are we going? J Biol Inorg Chem 2014; 19(2): 127–131.
5. Solomon I. Relaxation processes in a system of two spins. Phys Rev 1955; 99: 559–565.
6. Bloembergen N. Proton relaxation times in paramagnetic solutions. J Chem Phys 1957; 27: 572–573.
7. Bloembergen N, Morgan LO. Proton relaxation times in paramagnetic solutions. Effects of electron spin relaxation. J Chem Phys 1961; 34: 842–850.
8. Powell DH, Ni Dhubhgaill OM, Pubanz D, Helm L, Lebedev YS, Schlaepfer W, Merbach AE. High-pressure NMR kinetics. Part 74. Structural and dynamic parameters obtained from O-17 NMR, EPR, and NMRD studies of monomeric and dimeric Gd^{3+} complexes of interest in magnetic resonance imaging: an integrated and theoretically self-consistent approach. J Am Chem Soc 1996; 118(39): 9333–9346.
9. Freed JH. Dynamic effects of pair correlation functions on spin relaxation by translational diffusion in liquids. II. Finite jumps and independent T_1 processes. J Chem Phys 1978; 68(9): 4034–4037.
10. Helm L. Relaxivity in paramagnetic systems: theory and mechanism. Prog Nucl Magn Reson Spectrosc 2006; 49(1): 45–64.
11. Costa J, Ruloff R, Burai L, Helm L, Merbach AE. Rigid $M^{II}L_2Gd_2^{III}$ (M = Fe, Ru) complexes of a terpyridine-based heteroditopic chelate: a class of candidates for MRI contrast agents. J Am Chem Soc 2005; 127(14): 5147–5157.
12. Rast S, Fries PH, Belorizky E, Borel A, Helm L, Merbach AE. A general approach to the electronic spin relaxation of Gd(III) complexes in solutions. Monte Carlo simulations beyond the Redfield limit. J Chem Phys 2001; 115(16): 7554–7563.
13. Swift TJ, Connick RE. NMR (nuclear magnetic resonance)-relaxation mechanisms of O-17 in aqueous solutions of paramagnetic cations and the lifetime of water molecules in the first coordination sphere. J Chem Phys 1962; 37: 307–320.
14. Leigh JS Jr. Relaxation times in systems with chemical exchange. Exact solutions. J Magn Reson 1971; 4(3): 308–311.
15. Dunand FA, Borel A, Helm L. Gd(III) based MRI contrast agents: improved physical meaning in a combined analysis of EPR and NMR data? Inorg Chem Commun 2002; 5(10): 811–815.
16. Powell DH, Merbach AE, González G, Brücher E, Micskei K, Ottaviani MF, Köhler K, Von Zelewsky A, Grinberg OY, Lebedev YS. Magnetic-field-dependent electronic relaxation of Gd^{3+} in aqueous solutions of the complexes $[Gd(H_2O)_8]^{3+}$, $[Gd(propane\text{-}1,3\text{-}diamine\text{-}N,N,N',N'\text{-}tetraacetate})(H_2O)_2]^-$, and [Gd(N,N′-bis[(N-methylcarbamoyl)methyl]-3-azapentane-1,5-diamine-3,N,N′-triacetate)(H_2O)] of interest in magnetic-resonance imaging. Helv Chim Acta 1993; 76(5): 2129–2146.
17. Vander Elst L, Sessoye A, Laurent S, Muller RN. Can the theoretical fitting of the proton-nuclear-magnetic-relaxation-dispersion (proton NMRD) curves of paramagnetic complexes be improved by independent measurement of their self-diffusion coefficients? Helv Chim Acta 2005; 88(3): 574–587.
18. Micskei K, Helm L, Brücher E, Merbach AE. O-17 NMR study of water exchange on $[Gd(DTPA)(H_2O)]^{2-}$ and $[Gd(DOTA)(H_2O)]^-$ related to NMR imaging. Inorg Chem 1993; 32(18): 3844–3850.
19. Dunand FA, Borel A, Merbach AE. How does internal motion influence the relaxation of the water protons in Ln(III)DOTA-like complexes? J Am Chem Soc 2002; 124(4): 710–716.
20. Halle B, Wennerström H. Nearly exponential quadrupolar relaxation. A perturbation treatment. J Magn Reson 1981; 44(1): 89–100.
21. Yazyev OV, Helm L. ^{17}O nuclear quadrupole coupling constants of water bound to a metal ion: a gadolinium(III) case study. J Chem Phys 2006; 125(5): 054503/054501–054503/054508.
22. Whitley D. An overview of evolutionary algorithms practical issues and common pitfalls. Inf Softw Technol 2001; 43: 817–831.
23. Peters JA, Huskens J, Raber DJ. Lanthanide induced shifts and relaxation rate enhancements. Prog Nucl Magn Reson Spectrosc 1996; 28: 283–350.
24. Peters JA, Djanashvili K, Geraldes CFGC, Platas-Iglesias C. Structure, Dynamics, and Computational Studies of Lanthanide-Based Contrast Agents. Wiley: Chichester UK, 2013; 209–276.
25. Beeby A, Clarkson IM, Dickins RS, Faulkner S, Parker D, Royle L, de Sousa AS, Williams JAG, Woods M. Non-radiative deactivation of the excited states of europium, terbium and ytterbium complexes by proximate energy-matched OH, NH and CH oscillators: an improved luminescence method for establishing solution hydration states. J Chem Soc Perkin Trans 2 1999; 3: 493–504.
26. Graeppi N, Powell DH, Laurenczy G, Zekany L, Merbach AE. Coordination equilibria and water exchange kinetics of lanthanide(III) propylenediaminetetraacetates and other magnetic resonance imaging related complexes. Inorg Chim Acta 1995; 235: 311–326.
27. Tóth É, Ni Dhubhghaill OM, Besson G, Helm L, Merbach AE. Coordination equilibrium – a clue for fast water exchange on potential magnetic resonance imaging contrast agents? Magn Reson Chem 1999; 37(10): 701–708.
28. Yerly F, Dunand FA, Tóth É, Figueirinha A, Kovacs Z, Sherry AD, Geraldes CFGC. Spectroscopic study of the hydration equilibria and water exchange dynamics of lanthanide(III) complexes of 1,7-bis(carboxymethyl)-1,4,7,10- tetraazacyclododecane (DO2A). Eur J Inorg Chem 2000; 5: 1001–1006.
29. Balogh E, Mato-Iglesias M, Platas-Iglesias C, Tóth É, Djanashvili K, Peters JA, de Blas A, Rodriguez-Blas T. Pyridine- and phosphonate-containing ligands for stable Ln complexation. Extremely fast water exchange on the Gd^{III} chelates. Inorg Chem 2006; 45(21): 8719–8728.
30. Caravan P, Astashkin AV, Raitsimring AM. The gadolinium(III)–water hydrogen distance in MRI contrast agents. Inorg Chem 2003; 42(13): 3972–3974.
31. Astashkin AV, Raitsimring AM, Caravan P. Pulsed ENDOR study of water coordination to Gd^{3+} complexes in orientationally disordered systems. J Phys Chem A 2004; 108(11): 1990–2001.
32. Regueiro-Figueroa M, Platas-Iglesias C. Toward the prediction of water exchange rates in magnetic resonance imaging contrast agents: a density functional theory study. J Phys Chem A 2015; 119(24): 6436–6445.

SUPPORTING INFORMATION

Additional supporting information can be found in the online version of this article at the publisher's website.